Comm. Korean Math. Soc. **16** (2001), No. 3, pp. 459–485

ELECTRICAL IMPEDANCE IMAGING FOR SEARCHING ANOMALIES

OHIN KWON, JIN KEUN SEO, EUNG JE WOO*, AND JEONG-ROCK YOON

ABSTRACT. The aim of EIT (electrical impedance tomography) system is to image cross-sectional conductivity distribution of a human body by means of both generating and sensing electrodes attached onto the surface of the body, where currents are injected and voltages are measured. EIT has been suffered from the severe ill-posedness which is caused by the inherent low sensitivity of boundary measurements to any changes of internal tissue conductivity values. With a limited set of current-to-voltage data, figuring out full structure of the conductivity distribution could be extremely difficult at present time, so it could be worthwhile to extract some necessary partial information of the internal conductivity. We try to extract some key patterns of current-to-voltage data that furnish some core information on the conductivity distribution such as location and size. This overview provides our recent observation on the location search and the size estimation.

1. Introduction

Electrical impedance imaging system is designed to reconstruct resistivity (or conductivity) image of a subject using injected currents and voltage measurements. In electrical impedance imaging, a chain of electrodes is attached onto the surface of a conducting body, where different current patterns are applied and their corresponding voltage potentials are measured. Imaging the electrical conductivity distribution of an object by this system has been received considerable attention due to

Received May 1, 2001.

2000 Mathematics Subject Classification: 35R30, 62P30, 65N21.

Key words and phrases: inverse conductivity problem, anomaly detection, location and size estimation.

*The author was supported by grant No. 2000-2-31400-008-3 from the Basic Research Program of KOSEF.

its low cost and possible applications in medical imaging, corrosion detection, crack detection, etc. However, static EIT imaging is still far from clinical applications because of the severe ill-posedness which is caused by the inherent low sensitivity of boundary measurements to any changes of internal tissue conductivity values. Moreover, EIT has highly nonlinear relation between the target (conductivity distribution) and the current-voltage data. So, EIT has quite different nature from CT (computerized tomography) and MRI (magnetic resonance imaging) which have linear relation between the target image value and the observed data obtained by X-ray or NMR (nuclear magnetic resonance) signal.

The electrical impedance imaging system can be modeled by an elliptic partial differential equation. Suppose that an electrically conducting body, whose conductivity distribution is to be reconstructed, is occupied in a region $\Omega \subset \mathbb{R}^n (n = 2, 3)$. The conductivity, denoted by σ, is assumed to be a symmetric, positive definite matrix which has jump across an interface between different regions. Across the interface, the normal component of the electric field and the tangential component of the current density are discontinuous. Our goal is to identify this interface considering the above jump relation carefully.

For simplicity, let us assume σ to be a scalar valued function, which occurs in isotropic conducting media. When we inject a current, denoted by a function g on $\partial\Omega$, into the subject, electric current density $\mathbf{J}$ will be set up within the object satisfying $-\mathbf{J} \cdot \nu|_{\partial\Omega} = g$ where ν denotes the outward unit normal vector to the boundary. Since $\mathbf{J} = -\sigma\nabla u$ where u is the voltage potential, after normalization, u is governed by the following Neumann problem

$$\begin{aligned} \operatorname{div}\left(\sigma\nabla u\right) &= 0 \quad \text{in } \Omega, \\ \sigma\frac{\partial u}{\partial \nu} &= g \quad \text{on } \partial\Omega, \quad \text{and} \quad \int_{\partial\Omega} u\, ds = 0. \end{aligned}$$

It is well known that, for a given $g \in H^{-1/2}(\partial\Omega)$ satisfying an appropriate compatibility condition, the above Neumann problem has a unique solution in $H^1(\Omega)$. From now on, we denote the solution u of the Neumann problem by $u[\sigma, g]$ because it is determined uniquely by the conductivity distribution σ and the Neumann data g.

To get better information on the target image σ, we may apply several currents g_j, $j = 1, \cdots, N$ and measure the corresponding boundary voltages $f_j := u[\sigma, g_j]|_{\partial\Omega}$. In practice, the number N of possible applied currents is limited due to the finite number of attached electrodes.

The inverse problem of reconstructing σ is to invert the highly nonlinear map $T : \mathcal{C} \to [L^2(\partial\Omega)]^N$ defined by

$$T(\sigma) = \mathbf{f} := (f_1, f_2, \cdots, f_N)$$

where $\mathcal{C}$ is a set of all possible conductivity σ. To search $T^{-1}(\mathbf{f})$, it is necessary to interpret how the change in conductivity affect the current-to-voltage relation. Also, it should be taken account into inevitable noise in measurements and modeling errors. Indeed, since the data $\mathbf{f}$ always is distorted by some measurement error, we seek an approximate solution which is selected out of the set

$$\mathcal{C}_\epsilon[\mathbf{f}] := \{\sigma \in \mathcal{C} : \|T(\sigma) - \mathbf{f}\|_{L^2(\partial\Omega)} \leq \epsilon := \text{a given noise level}\}.$$

In order that an approximate solution is close to a true solution, the diameter of the set $\mathcal{C}_\epsilon[\mathbf{f}]$ should be reasonably small in some appropriately chosen metric. The diameter $\mathcal{C}_\epsilon[\mathbf{f}]$ is large when small perturbations of data cause large distortions to the solution in a given metric. What could be an appropriate admissible class $\mathcal{C}$ and reasonable metric? Considering all possible conductivity distribution σ of the human body, it is reasonable to assume that the admissible class $\mathcal{C}$ is contained in the set of all positive piecewise C^1–functions. As a metric for $\mathcal{C}$, a metric involving total variation and the standard $H^1(\Omega)$-norm could be effective to distinguish discontinuous images. Once a metric is fixed, the diameter $\mathcal{C}_\epsilon[\mathbf{f}]$ depends on the choice of $\mathcal{C}$ and applied current pattern g. To reduce the diameter of $\mathcal{C}_\epsilon[\mathbf{f}]$, unnecessary functions should be excluded from the admissible class $\mathcal{C}$ using *a priori* information about the physical structure of the body so that in a small class $\mathcal{C}$ the size of $\mathcal{C}_\epsilon[\mathbf{f}]$ could be shrunk significantly. Choice of applied currents also plays an important role on the size of $\mathcal{C}_\epsilon[\mathbf{f}]$. For example, highly oscillatory current-voltage data usually give poor information on the presence of anomalies lying in deep inside body because most of currents flow near the boundary.

Let us focus on a simple model such as the case of piecewise constant conductivity. Suppose that $\mathcal{C}$ is the set of σ which is of the form

$$\sigma = \sigma_0 \chi_{\Omega \setminus \bigcup_{j=1}^M \bar{D}_j} + \sum_{j=1}^M \sigma_j \chi_{D_j}$$

where M is a natural number, σ_0, σ_j are positive constants and D_j are smooth domains contained in Ω, and χ_D denotes the characteristic function of D. We assume that the diameter of $\mathcal{C}_\epsilon[\mathbf{f}]$ is reasonably small

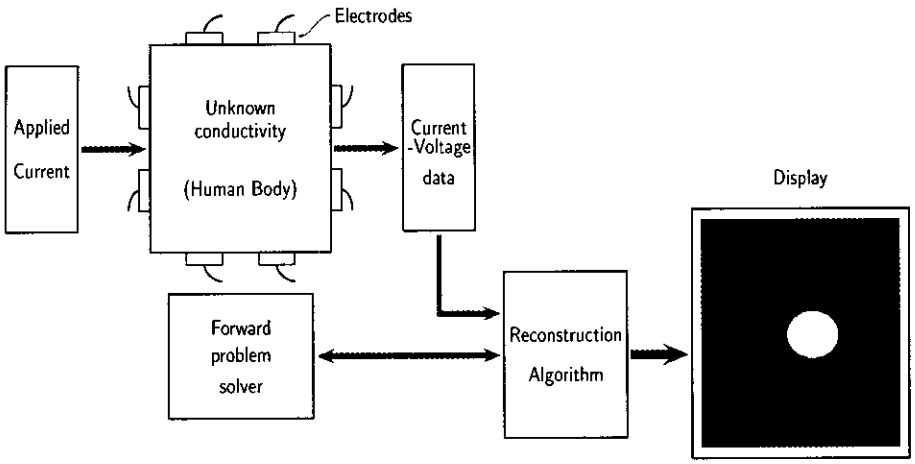

FIGURE 1. EIT schematic diagram.

for appropriately chosen currents, although we do not have any mathematical evidence. Then, our question is how to find one out of $\mathcal{C}_\epsilon[\mathbf{f}]$ numerically with economical value. Most of reconstruction processes use iterative schemes which require to solve the forward problem for each change of the conductivity until the calculated boundary voltages $T(\sigma)$ are matched to the measured voltages $\mathbf{f}$ within a noise level ϵ. In these methods, reconstruction algorithms require tremendous computational time and its iteration scheme may fail to converge to an approximate solution without taking a good initial guess. In our knowledge at present, it is too laborious to develop instant reconstruction algorithm for the full bulk shape of D_j. Instead, it could be worthwhile to extract only necessary partial information of D_j such as location and size. This paper deals with both the mathematical theory and the numerical algorithm for these aspects.

2. Tomography

The most common tomography, which is making cross-sectional views of an object, is the X-ray Computerized Tomography(CT) which uses multiple X-ray projection images, each from different angle. A photographic film generated by X-ray projection is an aggregated image where each pixel's brightness presents the X-ray absorption ratio across the section of the object. CT system collect two-dimensional projections of a three dimensional body by rotating X-ray source with a detector in

parallel and opposing direction, pivoting about the slice image of interest. Let us denote by $\rho(x,y)$ the attenuation function which represents the CT slice image of interest. X-ray projection of two-dimensional image $\rho(x,y)$ taken from an angle $\theta+\pi/2$ is the one-dimensional function $X_\theta\rho(t)$ which is calculated from the line integral through the line $\{x\cos\theta+y\sin\theta=t\}$:

$$X_\theta\rho(t) := \int_{\{x\cos\theta+y\sin\theta=t\}} \rho(x,y)\,dl.$$

The projection map X_θ from the density is linear and the reconstruction formula of the target image ρ from the known data $X_\theta\rho(t), 0<\theta<\pi$, is derived by inverse Fourier transform with the identity

$$\begin{aligned}\mathcal{F}_1[X_\theta\rho](\omega) &= \int_{-\infty}^{\infty} X_\theta\rho(t)e^{-i\omega t}dt \\ &= \int_{-\infty}^{\infty}\int_{-\infty}^{\infty} \rho(x,y)e^{-i\omega(x\cos\theta+y\sin\theta)}dxdy \\ &= \mathcal{F}_2[\rho](\omega\cos\theta,\omega\sin\theta)\end{aligned}$$

where $\mathcal{F}_1$ is the one dimensional Fourier transform and $\mathcal{F}_2$ is the two dimensional Fourier transform. Precisely, the density ρ can be obtained explicitly by the formula

$$\rho(x,y)=\frac{1}{4\pi^2}\int_0^{\infty}\int_0^{2\pi}\left(\int_{-\infty}^{\infty} X_\theta\rho(t)e^{-i\omega t}dt\right)\omega e^{i\omega(x\cos\theta+y\sin\theta)}d\theta d\omega.$$

Although CT creates excellent spatial resolution using discrete X-ray projection $X_{\theta_j}\rho, j=1,\cdots,m$, we are reluctant to use it due to the possible damage of tissue by X-rays.

Another important one in medical diagnostic imaging is Magnetic Resonance Imaging(MRI) where the distribution of the hydrogen atoms in the body placed within a large, changing magnetic field is imaged by measuring the radio-frequency emissions of the molecules in response to the changing magnetic fields. The human body is primarily composed of fat and water which have many hydrogen atoms and hydrogen nuclei have an NMR signal. After demodulating the NMR signal, the signal can be written by

$$\mathrm{S}(t_x,t_y,t_z)=\int \rho(x,y,z)\exp[-i\gamma(x\mathrm{G}_x t_x+y\mathrm{G}_y t_y+z\mathrm{G}_z t_z)]dxdydz,$$

where $\mathrm{S}(t_x,\ t_y,\ t_z)$ is the NMR signal expressed in 3-dimensional data acquisition axes t_x,t_y,t_z, $\rho(x,y,z)$ is the nuclear spin density, γ is the gyromagnetic ratio and G_x, G_y, G_z are the gradient field strengths.

Therefore like CT image the density image $\rho(x, y, z)$ can be obtained by inverse Fourier transform.

What about EIT? Unlike CT and MRI, EIT does not have such a nice inversion formula. In CT and MRI, there is a linear relation between the target density ρ and data such as X-ray projections or NMR signals. That is, the data corresponding to $\rho_1 + \rho_2$ is sum of the two data corresponding to $\rho_i, i = 1, 2$. However, EIT does not have such a nice linearity property because electric current is distorted by global structure of the conductivity σ. Therefore the reconstruction technique in CT and MRI cannot be applied to EIT.

3. EIT system for experiments

EIT requires a way to inject different patterns of currents and measure voltages using a set of electrodes attached on the boundary of a subject. It is more desirable to use separate electrodes for current injection and voltage measurement in order to avoid the effects of electrode-skin contact impedance. Therefore, we use a compound electrode which consists of a small voltage measuring electrode surrounded by a large current injection electrode separated by a small gap. Each current injection electrode is connected to a current source whose output is 50kHz sinusoid with variable amplitude. We can safely inject more amount of current as we increase the frequency. On the other hand, it is more difficult to handle high-frequency signals due to various stray capacitances throughout the EIT system and the subject. Therefore, we choose 50kHz as the optimal operating frequency for our EIT system.

We developed a computer-controlled EIT system including 32 independent current sources, two analog multiplexers for the selection of a pair of voltage measuring electrodes, voltage measuring circuits with a narrow-band variable-gain ac amplifier and a phase-sensitive demodulator, and a 12-bit A/D converter. After we attach 32 compound electrodes around the boundary of a subject, we can inject different patterns of current through current injection electrodes. Boundary voltage data on each voltage measuring electrode is sequentially measured using the EIT system. The entire circuitry of the EIT system is tuned so that the performance reaches the overall accuracy of ± 1-bit from the full scale of 12-bit. This means that the total measurement error is within 0.049% of full scale. We plan to upgrade the EIT system using 16-bit A/D converter and improve analog circuitry to further reduce the total measurement error. We constructed two circular phantoms. One is equipped

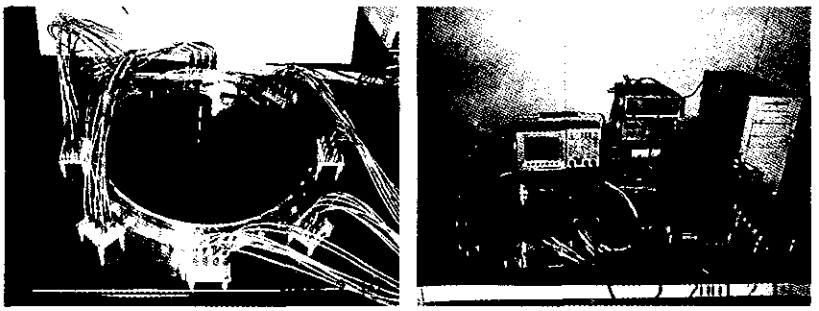

(a) (b)

FIGURE 2. EIT phantoms : (a) A phantom with 32 electrodes attached, (b) A phantom connected to EIT system with shielded coaxial cables.

with 16 compound electrodes and the other has 32 compound electrodes (Figure 2 (a)). We use shielded coaxial cables for the connection between electrodes and the EIT system to minimize the measurement error due to stray capacitances and external noise (Figure 2 (b)). We fill the phantom with electrolyte solution with known conductivity. Anomalies with different conductivity values and shapes are placed inside the phantom. Boundary current-voltage data from the phantom is used to reconstruct the conductivity distribution of the phantom. After we verify the performance of the EIT system using phantoms, we plan to develop electrode applicators for human subjects.

4. Location search and size estimation

We consider an inverse problem for finding the anomaly of discontinuous electrical conductivity by one current-voltage observation. Difficulties of this problem are due to its inherent ill-posedness and nonlinearity. Many authors proposed various reconstruction algorithms, most of which are based on laborious least square algorithms and Newton-type iteration schemes. In these methods, one has to take a good initial guess *a priori*. Without taking a good initial guess, to identify the conductivity distribution seems to be pessimistic: One needs tremendous computational costs and time to get a close image to the true solution, since Newton-type iteration schemes may not converge to an approximate solution unless the initial guess is close to the true solution. Evidently,

success or failure of Newton-type procedures heavily depend on how one can take a good initial guess.

In the papers [19, 20], a real time algorithm has been developed to determine the location and the size of the anomaly. In this real time method, the location of anomalies is immediately determined from the pattern of a simple weighted combination of the input current and the output voltage. And the size estimation is accomplished by simply calculating the Joule's energy integral. Combining two algorithms, we could take a good initial guess for the inverse conductivity problem for piecewise constant conductivity distributions. Moreover, both algorithms are stable and within real time (the combined algorithm takes less than one second).

Our model under consideration is an electrically conducting body of the form

$$\sigma(x) = 1 + \mu\chi_D(x) \qquad (-1 < \mu \neq 0 < \infty),$$

where D may be multiply connected. Then the relationship between the applied current g across the boundary $\partial\Omega$ and the corresponding measured voltage potential $f := u|_{\partial\Omega}$ on $\partial\Omega$ is determined by solving the Neumann problem:

$$\begin{aligned} &\operatorname{div}\Big((1+\mu\chi_D)\nabla u\Big) = 0 \quad \text{in } \Omega, \\ &\frac{\partial u}{\partial \nu} = g \quad \text{on } \partial\Omega, \ ; \text{ and } \int_{\partial\Omega} u\, ds = 0. \end{aligned} \tag{4.1}$$

The inverse problem with one measurement is to determine D from one pair of data (g, f). For some related results, please refer to [1, 4, 5, 6, 7, 8, 9, 10, 11, 12, 13, 14, 15, 16, 17].

4.1. Representation formula

The location search algorithm is based on simple aspects of the function $H(\cdot; g, f)$ which is computed directly from the data g and f,

$$H(x; g, f) := \int_{\partial\Omega} \frac{\partial\Phi(x-y)}{\partial\nu(y)} f(y)\, ds_y - \int_{\partial\Omega} \Phi(x-y) g(y)\, ds_y, \quad x \in \mathbb{R}^n \backslash \partial\Omega, \tag{4.2}$$

where Φ is the fundamental solution of Laplacian given by

$$\Phi(x-y) := \begin{cases} \dfrac{1}{2\pi} \log|x-y| & \text{for } n = 2, \\ \dfrac{-1}{4\pi} \dfrac{1}{|x-y|} & \text{for } n = 3. \end{cases}$$

To get an inspirational insight, we first investigate how the domain D is related to the Cauchy data (f, g) by means of the Neumann problem (4.1). Let us start with a basic identity

$$\int_\Omega \Delta\Phi(x-y)u(y)dy = \begin{cases} u(x) & \text{for } x \in \Omega, \\ 0 & \text{for } x \in \mathbb{R}^n \setminus \bar{\Omega}, \end{cases}$$

when the left integration is understood in a distributional sense.

By integrating by parts and using the transmission boundary condition on ∂D (the tangential component of the electric field $E = -\nabla u$ is continuous across the boundary ∂D, while its normal component has a jump with

$$\frac{\partial u_+}{\partial \nu} = (1+\mu)\frac{\partial u_-}{\partial \nu} \qquad \text{on} \quad \partial D,$$

where $u_- := u|_D$ and $u_+ := u|_{\Omega\setminus\bar{D}}$), we get

$$H(x,g,f) + \mu \int_D \nabla_y \Phi(x-y) \cdot \nabla u(y)dy = \begin{cases} u(x) & \text{for } x \in \Omega, \\ 0 & \text{for } x \in \mathbb{R}^n \setminus \bar{\Omega}. \end{cases}$$

Then our inverse problem is reduced to determine D from the known function $H(x; g, f)$.

Reduced inverse problem. *Find D so that*

$$\mu \int_D \nabla_y \Phi(x-y) \cdot \nabla u(y)dy = -H(x,g,f), \quad x \in \mathbb{R}^n \setminus \bar{\Omega}. \tag{4.3}$$

In this formulation, our search domain D is still complicatedly related to the observation data H, because ∇u in the integrand depends nonlinearly on D again. One possible way to remove an unknown u has been proposed in [16]: Using layer potential techniques and the integration by parts, the left hand side of (4.3) is converted into the following boundary integral which is determined by only one unknown D and the known information $H(\cdot, g, f)$ as follows:

$$\begin{aligned} & \mu \int_D \nabla_y \Phi(x-y) \cdot \nabla u(y)dy \\ = \; & \mathcal{S}_D \left\{ \left(\frac{2+\mu}{2\mu} I + \mathcal{K}_D^* \right)^{-1} \left. \frac{\partial H}{\partial \nu} \right|_{\partial D} \right\}(x) \quad \text{for } x \in \mathbb{R}^n \setminus \bar{\Omega}, \end{aligned}$$

where $\mathcal{S}_D$ and $\mathcal{K}_D^*$ are given by

$$\mathcal{S}_D\phi(x) = \int_{\partial D} \Phi(x-y)\phi(y)ds_y \quad \text{and} \quad \mathcal{K}_D^*\phi(x) = \int_{\partial D} \frac{\partial \Phi(x-y)}{\partial \nu_x}\phi(y)ds_y.$$

For the detailed description of the above formulation, please refer to [16].

4.2. Current flow structure

The location search algorithm and the size estimation algorithm are based on the observation of the structure of the current flow inside a body.

Figure 3 presents the resulting current flow by injecting current given by $g := \vec{e}_2 \cdot \nu$. The current flow is refracted across the interface between two different conductivity and the current seems to flow straight with the direction $\vec{e}_2$ on the included anomaly. In fact, this phenomena arise frequently in experiments and simulations. We utilize this phenomena later to determine the location and the size of the anomaly.

In Figure 3 (a) of a concentric disc case, the solution u to (4.1) is described by

$$u(\rho,\theta) = \begin{cases} \dfrac{2\rho\sin\theta}{(2+\mu)+\mu(r/R)^2} & \text{in } D, \\ \dfrac{(2+\mu)\rho\sin\theta}{(2+\mu)+\mu(r/R)^2} - \dfrac{\mu r^2}{(2+\mu)+\mu(r/R)^2}\dfrac{\sin\theta}{\rho} & \text{in } \Omega\setminus\bar{D}. \end{cases}$$

Then the gradient vector field on D is

$$\nabla u|_D = \frac{2\vec{e}_2}{(2+\mu)+\mu(r/R)^2}.$$

In the recent papers [19] and [20], we presented the following asymptotic formula for the current flow.

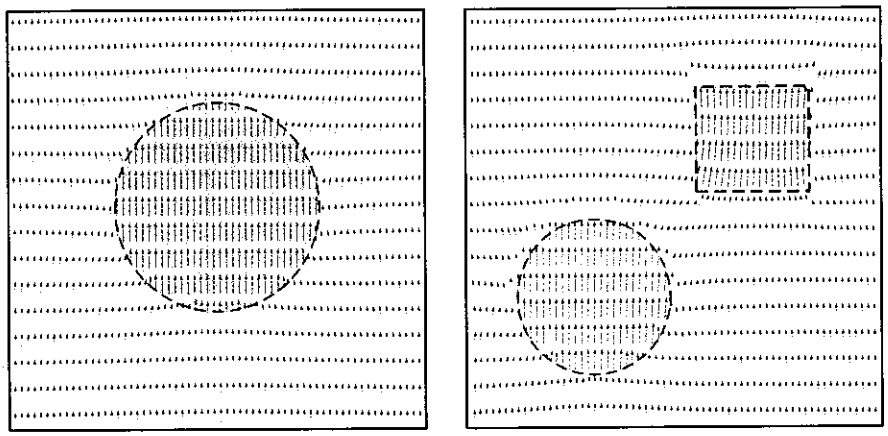

(a) (b)

FIGURE 3. Current flows in some conducting regions. The conductivity of shaded regions is two times greater than that of the background.

Straight current lemma.

LEMMA 4.1. *Let Ω be a C^2 domain in $\mathbb{R}^n$ and $g := \vec{a} \cdot \nu$ be given for a unit vector $\vec{a}$ as a Neumann data for (4.1). Suppose $D := \bigcup_{j=1}^{M} D_j$ satisfies that $D_j = B_{r_j}(z_j)$ with $r_j < \epsilon$, $\operatorname{dist}(D_j, D_k) > L$ for $j \neq k$, and $\operatorname{dist}(D_j, \partial\Omega) > L$ for all $j = 1, \cdots, M$, where ϵ and L are fixed positive numbers. Then the gradient vector field of the solution u for (4.1) on D is approximated by*

$$\nabla u(x) = \frac{n\vec{a}}{n+\mu} + O(\epsilon^2), \qquad x \in D.$$

The proof of the above lemma is based on the comparison between the solution u and the following function

$$v(x) = \vec{a} \cdot x + \frac{n\mu}{n+\mu} \sum_{j=1}^{M} \int_{D_j} \nabla_y \Phi(x-y) \cdot \vec{a}\, dy + c,$$

where $\Phi(x-y)$ is the fundamental solution of the Laplacian and the constant c is chosen so that $\int_{\partial\Omega} v\, ds = 0$. Then v is the solution to the

conductivity equation (4.1) with a slightly perturbed Neumann data $\tilde{g}$. Using singular integral estimate, it can be shown that

$$\nabla u(x) = \nabla v(x) + O(\epsilon^2), \qquad x \in \Omega,$$

and for $k = 1, \cdots M$,

$$\nabla v(x)$$

$$= \frac{2\vec{a}}{\mu+2} + \frac{\mu}{\mu+2} \sum_{j \neq k}^{M} \left(\frac{r_j}{|x - z_j|} \right)^2 \left(\frac{2\vec{a} \cdot (x - z_j)}{|x - z_j|^2} (x - z_j) - \vec{a} \right), \quad x \in D_k,$$

for $n = 2$ and similar results can be also obtained for $n = 3$. For more details, refer to [19, 20]. The result in Lemma 4.1 is exactly what we have seen in Figure 3.

4.3. Joule's energy integral

In the electric circuit theory, it is well-known that the total power (work done per unit time) P_Γ of the circuit element $\Gamma := (a, b)$ is given by

$$P_\Gamma = [V(b) - V(a)] \times I,$$

where V and I denote the voltage at the point and the current flowing the cross section of Γ, respectively. This amount of energy is thus transmitted from the electric field to the atoms in thermal vibration per unit time.

Generally, the total power P_Ω converted into heat for a domain $\Omega \subset \mathbb{R}^n$ is given by the following Joule's energy integral

$$P_\Omega = \int_\Omega E(x) \cdot J(x)\, dx,$$

where E and J denote the electric field intensity and the current density vector, respectively.

When the physical situation is described by the conductivity equation (4.1) for given D and g, we have $E = -\nabla u$ and $J = -\sigma \nabla u$, where u is the solution to (4.1). Therefore we get

$$P_{\Omega,D} = \int_\Omega \sigma |\nabla u|^2\, dx = \int_{\partial\Omega} ug\, dx.$$

On the other hand, if there is no included anomaly, that is $D = \emptyset$, then the total power is given by

$$P_{\Omega,\emptyset} = \int_\Omega |\nabla U_0|^2\, dx = \int_{\partial\Omega} U_0 g\, dx,$$

where $U_0 = \vec{a} \cdot x$.

Physically, the difference of the powers

$$P_{\Omega,\emptyset} - P_{\Omega,D} = \int_{\partial\Omega} (U_0 - u) g \, dx \tag{4.4}$$

indicates the strength (mixed information of the size and the conductivity value (μ, D)) of the included anomaly. Moreover, the sign of the above integral reveals whether the included anomaly is conducting $(\mu > 0)$ or insulating$(\mu < 0)$.

Now we calculate the difference of the powers (4.4). Starting from the identity

$$0 = \int_D u \Delta U_0 \, dx + \int_{\Omega \setminus D} u \Delta U_0 \, dx,$$

we obtain

$$\int_{\partial\Omega} (U_0 - u) g \, ds = \int_{\partial D} \left(\frac{\partial u_+}{\partial \nu} - \frac{\partial u_-}{\partial \nu} \right) U_0 \, ds = \mu \int_{\partial D} \frac{\partial u_-}{\partial \nu} U_0 \, ds,$$

where $u_- := u|_D$ and $u_+ := u|_{\Omega \setminus \bar{D}}$. Using Green's identity, we finally achieve the following Joule's energy integral formula considering $\nabla U_0 = \vec{a}$.

Energy integral formula. The power difference is given by

$$P_{\Omega,\emptyset} - P_{\Omega,D} = \int_{\partial\Omega} (U_0 - u) g \, ds = \mu \int_D \nabla u \cdot \vec{a} \, dx. \tag{4.5}$$

4.4. Size estimation

Let us begin with upper and lower bound for the size of D:

$$\begin{aligned} & \frac{\min\{1, 1+\mu\}}{|\mu|} \left| \int_{\partial\Omega} (U_0 - u) g \, ds \right| \\ \leq\ & |D| \\ \leq\ & \frac{\max\{1, 1+\mu\}}{|\mu|} \left| \int_{\partial\Omega} (U_0 - u) g \, ds \right|. \end{aligned}$$

For the proof of the above estimate, please refer to [2, 3, 18]. In particular, Alessandrini, Rosset, and Seo [3] showed the optimal bound of size of inclusions for quite general g and σ.

In [19], Kwon and Seo developed an monotonicity algorithm for calculating the total size of anomalies. For simplicity, we will assume that $D \subset B_R(0) \subset \Omega$, and let $v_r \in H^1(\Omega)$ be the solution to the following

Neumann boundary value problem for the given current pattern $g := \vec{a}\cdot\nu$ where $\vec{a}$ is a fixed unit vector:

$$\begin{aligned} &\operatorname{div}\Big((1+\mu\chi_{B_r(0)})\nabla v_r\Big) = 0 \quad \text{in } \Omega, \\ &\frac{\partial v_r}{\partial \nu} = g \quad \text{on } \partial\Omega, \quad \text{and} \int_{\partial\Omega} v_r\, ds = 0. \end{aligned} \tag{4.6}$$

Then Kwon and Seo obtained the following monotonicity lemma.

LEMMA 4.2. *There exists a unique $r \in (0, R)$ so that*

$$\int_{\partial\Omega} (u - v_r) g\, ds = 0.$$

Then using the energy integral (4.5) and Lemma 4.1, we obtain

$$0 = P_{\Omega,D} - P_{\Omega,B_r(0)} = \int_{\partial\Omega} (u - v_r) g\, ds = \frac{n\mu}{n+\mu}\Big(|B_r(0)| - |D|\Big) + O(\epsilon^4).$$

Hence we obtain the following size estimation using monotonicity algorithm.

Monotonicity algorithm for size estimation. *The total size is approximately estimated by the measure of a ball centered at the origin*

$$|D| \approx |B_r(0)|,$$

where $r \in (0, R)$ is the unique number so that

$$\int_{\partial\Omega} (f - v_r) g\, ds = 0$$

for the measured voltage potential f corresponding to the applied current pattern $g := \vec{a}\cdot\nu$.

The above monotonicity algorithm can be improved by means of the following estimate

$$\int_{\partial\Omega} (U_0 - u) g\, ds = \frac{n\mu}{n+\mu}|D| + O(\epsilon^4),$$

which is obtained easily by a combination of the energy integral (4.5) and Lemma 4.1. As a consequence, we have the following energy integral algorithm.

Energy integral algorithm for size estimation. *The total size is approximately estimated by a simple energy integral*

$$|D| \approx \frac{n+\mu}{n\mu} \int_{\partial\Omega} (U_0 - f) g \, ds,$$

where f is the measured voltage potential corresponding to the applied current pattern $g := \vec{a} \cdot \nu$ and U_0 is the harmonic function with g as the Neumann data on $\partial\Omega$.

The energy integral algorithm, by which we need not solve any direct problem but calculate the simple integration, is really a real time algorithm. Moreover it is stable under the observation error contained in the measured voltage potential f, since we extract the information after integrating it. Figure 4 shows a numerical test for our energy integral algorithm for $\mu = 20$. The total area of 5 anomalies is given by 0.2827 and our estimation gives the value 0.2642.

4.5. Location search algorithm

Now we present the location search algorithm. We give justifications for two cases: Either when D is a small ball, or when the conductivity μ is close to zero without geometric restrictions on D. Though our numerical algorithm works satisfactorily for quite general cases of D

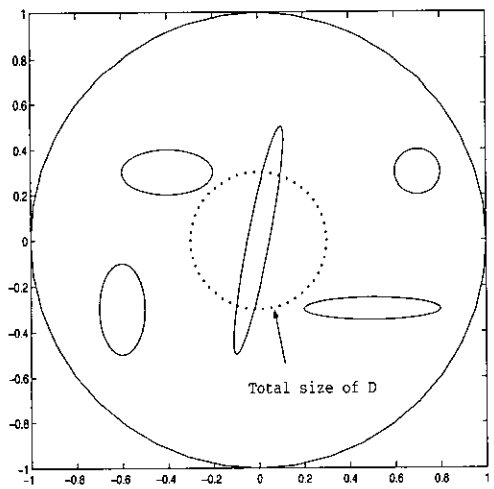

FIGURE 4. A numerical example for the size estimation algorithm.

and μ, the theoretical justifications are given for the restricted cases. Thus we expect these restrictions to be relaxed in the theoretical sense.

In case when the included anomaly is known to be a small ball $D := B_r(z)$, we can apply the straight current lemma (Lemma 4.1). Then the formulation (4.3) is reduced to

$$(4.7)\quad H(x;g,f) = \frac{\mu}{\omega_n(n+\mu)} \int_D \frac{(x-y)\cdot \vec{a}}{|x-y|^n}\, dy + O(\epsilon^4), \qquad x \in \mathbb{R}^n \setminus \bar{\Omega},$$

where ω_n denotes the volume of a unit ball in $\mathbb{R}^n$. By the fact that $D = B_r(z)$ is a ball, the mean value theorem for harmonic functions applied to the formulation (4.7) yields that

$$H(x;g,f) = \frac{\mu r^n}{n+\mu} \frac{(x-z)\cdot \vec{a}}{|x-z|^n} + O(\epsilon^4), \qquad x \in \mathbb{R}^n \setminus \bar{\Omega}.$$

Examining the function

$$\widetilde{H}(x;v) := \frac{\mu r^n}{n+\mu} \frac{(x-z)\cdot \vec{a}}{|x-z|^n},$$

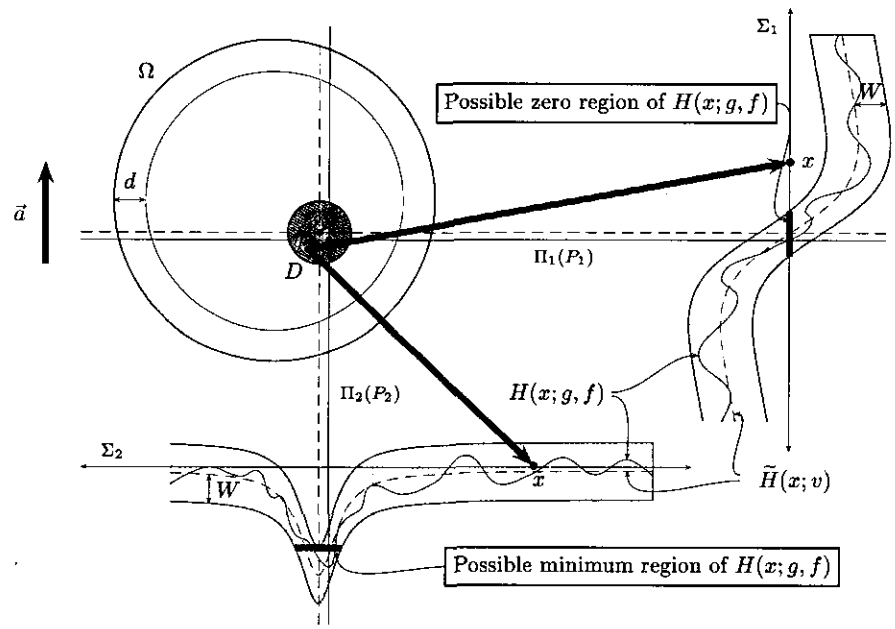

FIGURE 5. Relations between the location of the anomaly and the pattern of $H(x;g,f)$ in the case of $\mu > 0$.

we get an interesting observation: Take two observation regions Σ_1 and Σ_2 contained in $\mathbb{R}^3 \setminus \bar{\Omega}$, given by $\Sigma_1 :=$ a line parallel to $\vec{a}$ and $\Sigma_2 :=$ a plane normal to $\vec{a}$. Next we find two points $P_i \in \Sigma_i (i = 1, 2)$ so that $H(P_1; g, f) = 0$ and

$$H(P_2; g, f) = \begin{cases} \min_{x \in \Sigma_2} H(x; g, f) & \text{if } \mu > 0, \\ \max_{x \in \Sigma_2} H(x; g, f) & \text{if } \mu < 0. \end{cases}$$

Finally, we draw the corresponding plane $\Pi_1(P_1)$ and the corresponding line $\Pi_2(P_2)$ given by

$$\begin{aligned} & \Pi_1(P_1) := \{x \,|\, \vec{a} \cdot (x - P_1) = 0\} \\ \text{and} \quad & \Pi_2(P_2) := \{x \,|\, (x - P_2) \text{ is parallel to } \vec{a}\}. \end{aligned}$$

Then the intersecting point P of $\Pi_1(P_1) \cap \Pi_2(P_2)$ is close to the center of D.

Our algorithm gives a tool to determine one small anomaly, at least when it is a small perturbation of a ball. Figure 5 illustrates how the location search method works. Roughly speaking, the width function $W = W(x)$ of shaded region is proportional to r^4.

In case of an arbitrarily shaped domain having small conductivity $|\mu| << 1$, we compare $H(x; g, f)$ with

$$\widetilde{H}(x; U_0) := \frac{\mu}{n\omega_n} \int_D \frac{(x - y) \cdot \vec{a}}{|x - y|^n} \, dy.$$

Using standard Hölder estimate observing the difference $u - U_0$, we obtain the following estimate (see [20] for details)

$$H(x; g, f) = \widetilde{H}(x; U_0) + O(|\mu|^2), \quad x \in \mathbb{R}^n \setminus \bar{\Omega}.$$

Since the function $\widetilde{H}(x; U_0)$ possess the same property that we have required for the function $\widetilde{H}(x; v)$, we get the same conclusion as before.

Now we summarize the location search algorithm for a simply connected domain with constant conductivity and Figure 6 demonstrates the remarkable achievement of this algorithm.

Location search algorithm. *As an applied current pattern, we choose* $g(x) = \vec{a} \cdot \nu(x)$ *for some fixed constant vector* $\vec{a}$. *Take two observation regions* Σ_1 *and* Σ_2 *contained in* $\mathbb{R}^3 \setminus \bar{\Omega}$, *given by*

(4.8) $\Sigma_1 :=$ *a line parallel to* $\vec{a}$ *and* $\Sigma_2 :=$ *a plane normal to* $\vec{a}$.

Next we find two points $P_i \in \Sigma_i (i = 1, 2)$ *so that* $H(P_1; g, f) = 0$ *and*

$$H(P_2; g, f) = \begin{cases} \min\limits_{x \in \Sigma_2} H(x; g, f) & \text{if} \quad \mu > 0, \\ \max\limits_{x \in \Sigma_2} H(x; g, f) & \text{if} \quad \mu < 0. \end{cases}$$

Finally, we draw the corresponding plane $\Pi_1(P_1)$ *and the corresponding line* $\Pi_2(P_2)$ *given by*

$$\Pi_1(P_1) := \{x \,|\, \vec{a} \cdot (x - P_1) = 0\}$$
$$\text{and} \quad \Pi_2(P_2) := \{x \,|\, (x - P_2) \ \text{ is parallel to } \ \vec{a}\}.$$

Then the intersecting point P *of* $\Pi_1(P_1) \cap \Pi_2(P_2)$ *is close to the domain* D. *For two dimensional case, the same argument holds if one adjusts* Σ_2 *and* $\Pi_1(P_1)$ *to be simply lines in* $\mathbb{R}^2$.

When the anomaly is known to be of form

$$\sigma(x) := 1 + \mu(x),$$

where $\mu > 0$ is compactly supported by a simply connected domain D, we can extend the above location search algorithm to this case. The research is still in process. And moreover it is more worthwhile extending our location search algorithm to the case when D has many components. If we apply the oscillatory current pattern supported in a portion of the outer surface, the current will flow mainly near the surface. Using this pattern, we can detect the existence of the anomaly near that portion. This local search algorithm is also in preparation [21].

Before concluding this section we give a comment on the stability of the location search algorithm. In general, the measured voltage potential f_m contains the unavoidable observation noise, so that we have to answer the stability question. Fortunately, our location search algorithm is totally based on the observation of the pattern of $H(x; g, f)$, we have the following stability.

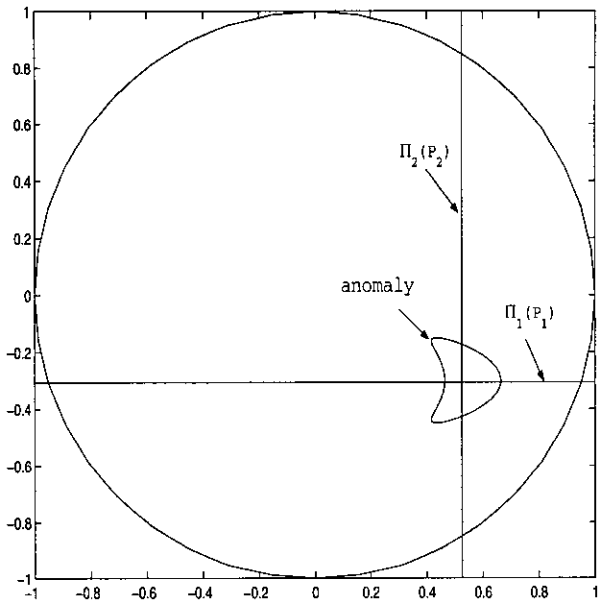

FIGURE 6. Location detection intersecting the lines $\Pi_1(P_1)$ and $\Pi_2(P_2)$.

REMARK 4.3. For $x \in \mathbb{R}^n \setminus \bar{\Omega}$, by the definition of $H(x; g, f_m)$ and $H(x; g, f)$ given in (4.2) we obtain

$$|H(x;g,f_m) - H(x;g,f)| = \left| \int_{\partial\Omega} \frac{\partial\Phi(x-y)}{\partial\nu(y)} \{f_m - f\}(y)\, ds_y \right| \tag{4.9}$$

$$\leq C \| f_m - f \|_{L^2(\partial\Omega)},$$

where C is a constant depending only on the distance of x from $\partial\Omega$. Thus we conclude that our location search algorithm is not sensitive to the observation noise.

5. Numerical reconstruction

5.1. Reconstruction algorithm

We now proceed with describing the application of Newton's method for solving the nonlinear equation

$$\mathcal{F}(\partial D) = f \tag{5.1}$$

for the unknown boundary ∂D of the included anomalies, where $f := u|_{\partial\Omega}$ is the measured voltage potential. Here u is the solution to the conductivity equation (4.1). To solve (5.1) by iterative methods, we consider the following linearized equation

$$\mathcal{F}(\partial D) + \mathcal{F}'(\partial D; h) = f \tag{5.2}$$

which we have to solve for h in order to improve an approximate boundary ∂D into a new approximation given by $\partial\tilde{D} = \partial D + h$. As usual, Newton's method consist in iterating this procedure.

The second term $\mathcal{F}'(\partial D; h)$ is expressed explicitly in the framework of domain derivative, which characterizes the perturbation of the solutions of a boundary value problem with respect to the variation of domains. The domain derivative approach has been introduced for various problems. In particular, Hettlich and Rundell [13] calculated the domain derivative as the following theorem.

THEOREM 5.1. *Let D be a subset of Ω of class C^2, $h \in C^2(\partial D; \mathbb{R}^n)$. Then the domain derivative $\mathcal{F}'(\partial D; h)$ is expressed by*

$$\mathcal{F}'(\partial D; h) = u'|_{\partial\Omega},$$

where u' solves the following boundary value problem

$$\Delta u' = 0 \quad \text{in } D \cup (\Omega \setminus \bar{D}),$$

with boundary conditions on $\partial\Omega$

$$\int_{\partial\Omega} u'\, ds = 0 \quad \text{and} \quad \frac{\partial u'}{\partial \nu} = 0,$$

and boundary conditions on ∂D

$$u'_+ - u'_- = -\mu(h \cdot \nu)\frac{\partial u_-}{\partial \nu},$$
$$(1+\mu)\frac{\partial u'_-}{\partial \nu} - \frac{\partial u'_+}{\partial \nu} = \mathrm{Div}_{\partial D}\Big((h \cdot \nu)\mathrm{Grad}_{\partial D} u\Big),$$

where $u_- := u|_D$, $u_+ := u|_{\Omega\setminus\bar{D}}$, $u'_- := u'|_D$, $u'_+ := u'|_{\Omega\setminus\bar{D}}$, and ν denotes the unit outward normal to $\partial\Omega$ or ∂D. Here $\mathrm{Div}_{\partial D}$ and $\mathrm{Grad}_{\partial D}$ denote the divergence and the gradient on the manifold ∂D.

Using the above theorem, we get the following Newton-type iteration reconstruction scheme.

Reconstruction strategy

(1) *Initial guess*: For the initial guess, we use our location search and the size estimation algorithm.
(2) *Forward problem*: For given boundary ∂D^n, the boundary value problem (4.1) for $D = D^n$ to obtain the solution u^n.
(3) *Evaluate of* $\mathcal{F}$: Then evaluate $\mathcal{F}(\partial D^n) := u^n|_{\partial\Omega}$.
(4) *Check and update*: If $||\mathcal{F}(\partial D^n) - f||_{L^2(\partial\Omega)} < \epsilon$ for some tolerance ϵ, stop; otherwise update the boundary as $\partial D^{n+1} := \partial D^n + h^n$, where the vector field h^n on ∂D^n is chosen so that the linearized equation (5.2) is satisfied in the least squares sense:

$$\mathcal{F}(\partial D^n) + \mathcal{F}'(\partial D^n; h^n) \approx f.$$

Go back to step (2).

5.2. Numerical simulation

In order to reconstruct the anomaly D, we use the previously mentioned Newton-type iterative scheme. With this method, selecting a good initial guess plays an important role. In general, the measured voltage potential f_m on $\partial\Omega$ contains an inevitable noise, which makes f_m different from the true voltage potential f on $\partial\Omega$. Then by the inherent ill-posed nature of inverse conductivity problem, we are not able to distinguish the delicate difference of shape of the anomaly D without having *a priori* information of D. That is, if one tries to reconstruct the shape of D with a blind initial guess, one deserves to consume a considerable time and to fall in the local minimum dilemma.

Fortunately, our location search and the size estimation algorithm are not only within real time, but also stable as seen in (4.9), so that we are able to give a stable initial guess. Having this well-chosen initial guess, we finally apply a Newton-type iterative scheme to reconstruct the anomaly D.

For a numerical simulation of our method, we consider the conducting body Ω as the unit disk centered at origin in $\mathbb{R}^2$. The applied current is given by $g := \vec{e}_2 \cdot \nu$ on $\partial\Omega$, that is

$$g(\theta) = \sin\theta, \quad \theta \in [0, 2\pi)$$

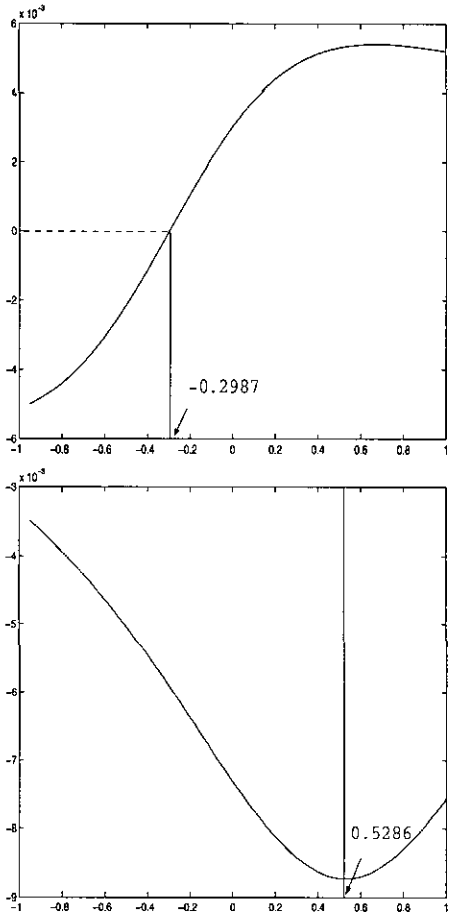

FIGURE 7. Patterns of $H(x; g, f_m)$ on the observation lines $\Sigma_1 = \{(1.5, s) \mid s \in \mathbb{R}\}$ and $\Sigma_2 = \{(s, -1.5) \mid s \in \mathbb{R}\}$.

and the anomaly D to be found is taken as a kite-shaped domain of conductivity $\mu = 5$, the boundary of which is parametrized as

$$\begin{aligned}\partial D &:= \{(x_1(t), x_2(t)) \\ &= (0.5 + 0.1\cos\theta + 0.065\cos 2\theta, -0.3 + 0.15\sin\theta) \mid 0 \le \theta < 2\pi\}.\end{aligned}$$

Since the numerical simulation is not an actual experiment, we need a direct solver which provides *output data*. To avoid invoking the inverse crime in numerical simulations, we must generate the *output* voltage potential $f := u|_{\partial\Omega}$ independent of our reconstruction algorithm. In this paper, we employ the method proposed in [7] to obtain f that has

nothing to do with our reconstruction algorithm. To reflect the practical situation, we assume the *measured* voltage potential f_m contains an observation error, which is given in our simulations by adding 3% random noise to f. Moreover, since the voltage potential can be detected only at the attached finite electrodes in practical situations, we assume that we have the data of f_m only at M equidistant points on $\partial\Omega$,

$$y_j := \left(\cos\frac{2j\pi}{M}, \sin\frac{2j\pi}{M}\right) \quad \text{for } j = 1, \ldots, M. \tag{5.3}$$

In our simulations we assume that we have attached 40 electrodes on $\partial\Omega$, i.e. $M = 40$.

First, we determine the location of an initial guess via our location search algorithm(Figure 5 serves an illustration.). Let the observation lines be given by $\Sigma_1 = \{(1.5, s) \,|\, s \in \mathbb{R}\}$ and $\Sigma_2 = \{(s, -1.5) \,|\, s \in \mathbb{R}\}$. Observing the function $H(x; g, f_m)$, which is obtained by a simple quadrature rule for (4.2) with data $\{g(y_j), f_m(y_j)\}_{j=1}^M$, we obtain the zero point $P_1 = (1.5, -0.2987)$ of $H(x; g, f_m)$ on Σ_1 and the minimum point $P_2 = (0.5286, -1.5)$ of $H(x; g, f_m)$ on Σ_2, noting that μ is positive. Figure 7 exhibits this procedure. Then the intersecting point P of $\Pi_1(P_1) \cap \Pi_2(P_2)$ in the location search algorithm is given by $P = (0.5286, -0.2987)$.

Next, we determine the size of the initial guess by two methods discussed in section 4.4. Using monotonicity algorithm, there exists the unique $r \in [0, 1)$ so that

$$T(r) := \left| \int_{\partial\Omega} (f_m - v_r) g \, ds \right| = 0,$$

where v_r is the solution to (4.6). Then the size of D is almost same as that of $B_r(0)$;

$$|\, D \,| \approx |\, B_r(0) \,|.$$

In order to solve $T(r) = 0$ approximately, we consider 20 points in $[0.025, 0.5]$ with the increment 0.025 and use an elementary quadrature rule: Find $r \in [0.025, 0.5]$ such that

$$\widetilde{T}(r) := \left| \sum_{j=1}^{M} \{f_m(y_j) - f_r(y_j)\} g(y_j) \right| = 0, \tag{5.4}$$

where $y_j \in \partial\Omega$ is given by (5.3).

Alternatively, using energy integral algorithm, we approximate the size of D by

$$|D| \approx \frac{2+\mu}{2\mu} \int_{\partial\Omega} (g - f_m) g \, ds,$$

since $U_0|_{\partial\Omega} = g$ in our setting. This energy integral algorithm is more efficient than the monotonicity algorithm, because we need not solve direct problems many times to find r for (5.4). However the estimated size by the monotonicity algorithm seems to be closer to the size of the unknown anomaly than the energy integral algorithm, the reason of which is still under investigation.

Figure 8 shows that the corresponding size of D is the ball $B_{0.125}(0)$ and represents the real shape of D and the remarkably selected initial guess.

Finally, using the above initial guess we reconstruct the anomaly D with Newton-type iterative scheme. Restricting the boundary curve ∂D to an admissible class $\mathcal{A}_N$ defined as a periodic parametrization,

$$\mathcal{A}_N := \Big\{ \Big(a_0 + \sum_{n=1}^{N} (a_n \cos nt + c_n \sin nt), b_0 + \sum_{n=1}^{N} (b_n \cos nt + d_n \sin nt) \Big) \Big| \; t \in [0, 2\pi] \Big\},$$

where the coefficients a_0, b_0 and a_i, b_i, c_i and d_i for $i = 1, \ldots, N$ are all real numbers, we update the approximation of the anomaly by reconstruction strategy. For step (4) in reconstruction strategy, we use the boundary integral formulation. See [13] for more details. For updating the approximation of the anomaly, we can also use Levenberg-Marquardt algorithm as demonstrated in [20].

If one has no *a priori* information on D, one has to begin with an arbitrarily chosen initial guess. Up to now, various methods have been developed without any *a priori* information on D. Even though their methods are working in a certain numerical process, they still have a large gab from the practical use of the EIT images. In our case, fortunately we obtained a good initial guess in the previous step. Thus with $B_{0.125}(P)$ as an initial guess we apply the above Newton-type iterative scheme. As seen in Figure 9, merely 6-iterations give a remarkable approximation of D, which is very hard to obtain with a blind initial guess even allowing much more iterations.

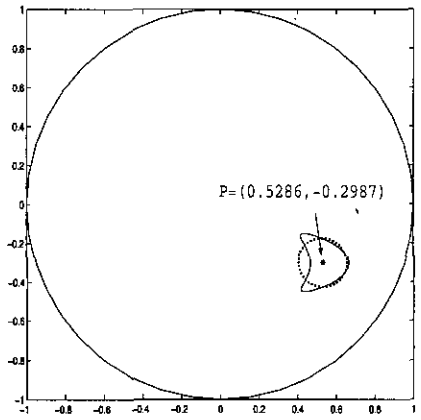

radius r	$\widetilde{T}(r)$
0.025	0.411620
0.050	0.385590
0.075	0.311471
0.100	0.200150
0.125	0.055389
0.150	0.121019
0.175	0.327338
0.200	0.562052
0.225	0.823650
0.250	1.110668
0.275	1.421805
0.300	1.756050
0.325	2.113455
0.350	2.504039
0.375	3.016947
0.400	2.694932
0.425	2.407876
0.450	2.245636
0.475	1.938697
0.500	0.683961

FIGURE 8. Solving (5.4) numerically and drawing the initial guess combining the estimated size with the previously determined location. The genuine area of the kite shaped domain is 0.136. The defect stems from the fact that the current flow in the kite shaped domain is not perfectly straight.

References

[1] G. Alessandrini, V. Isakov, and J. Powell, *Local uniqueness in the inverse problem with one measurement*, Trans. Amer. Math. Soc. **347** (1995), 3031–3041.

[2] G. Alessandrini and E. Rosset, *The inverse conductivity problem with one measurement: bounds on the size of the unknown object*, SIAM J. Appl. Math. **58** (1998), 1060–1071.

[3] G. Alessandrini, E. Rosset, and J. K. Seo, *Optimal size estimates for the inverse conductivity poblem with one measurement*, Proc. Amer. Math. Soc. **128** (2000), 53–64.

[4] H. Bellout and A. Friedman, *Identification problem in potential theory*, Arch. Rat. Mech. Anal. **101** (1988), 143–160.

[5] H. Bellout, A. Friedman, and V. Isakov, *Inverse problem in potential theory*, Trans. Amer. Math. Soc. **332** (1992), 271–296.

[6] M. Brühl and M. Hanke, *Numerical implementation of two non-iterative methods for locating inclusions by impedance tomography*, Inverse Problems **16** (2000), 1029–1042.

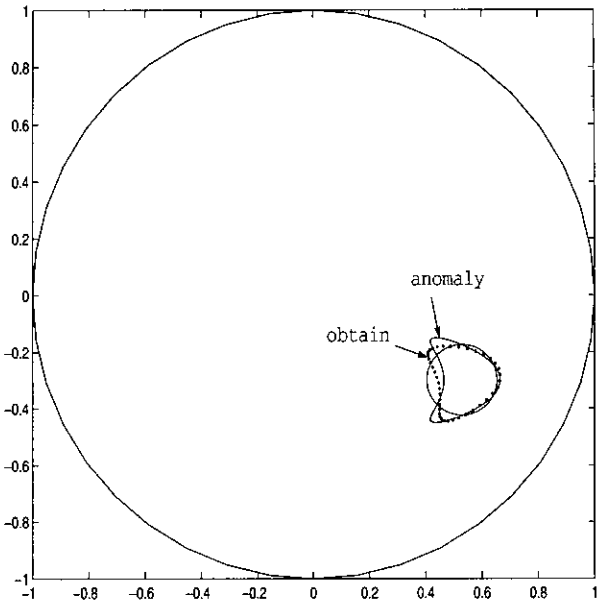

FIGURE 9. Approximation of the anomaly D after 6-iterations in case of $\mu = 5$ with 3% random noise in the voltage potential f_m. In this example, the value of cost functional is $\frac{1}{2}\| f_m - f_o \|^2_{L^2(\Omega)} = 4.226912 \times 10^{-6}$, denoting by f_o the voltage potential generated by the obtained anomaly.

[7] K. Bryan, *Numerical recovery of certain discontinuous electrical conductivities*, Inverse Problems **7** (1991), 827–840.

[8] D. J. Cedio-Fengya, S. Moskow, and M. Vogelius, *Identification of conductivity imperfections of small parameter by boundary measurements. Continuous dependence and computational reconstruction*, Inverse Problems **14** (1998), 553–595.

[9] M. Cheney, D. Isaacson, and J. C. Newell, *Electrical impedance tomography*, SIAM Review **41** (1999), 85–101.

[10] E. Fabes, H. Kang, and J. K. Seo, *Inverse conductivity problem: error estimates and approximate identification for perturbed disks*, SIAM J. of Math. Anal. **30** (1999), 699–720.

[11] A. Friedman and V. Isakov, *On the uniqueness in the inverse conductivity problem with one measurement*, Indiana Univ. Math. J. **38** (1989), 553–580.

[12] A. Friedman and M. Vogelius, *Identification of small inhomogeneities of extreme conductivity by boundary measurements: a theorem on continuous dependence*, Arch. Rat. Mech. Anal. **105** (1989), 299–326.

[13] F. Hettlich and W. Rundell, *The determination of a discontinuity in a conductivity from a single boundary measurement*, Inverse Problems **14** (1998), 67–82.

[14] P. Hua, W. Tompkins, and J. Webster, *A regularized electrical impedance tomography reconstruction algorithm*, Clin. Phys. Physiol. Meas. **9** (1988), 137–41.

[15] D. Isaacson, *Distinguishability of conductivities by electric current computed tomography*, IEEE Trans. Medical Imaging, (1986), pp. 91–95.

[16] H. Kang and J. K. Seo, *Layer potential technique for the inverse conductivity problem*, Inverse Problems **12** (1996), 267–278.

[17] ———, *Inverse conductivity problem with one measurement: uniqueness for balls in* $\mathbb{R}^3$, SIAM J. Appl. Math. **59** (1999), 1533–1539.

[18] H. Kang, J. K. Seo, and D. Sheen, *Inverse conductivity problem with one measurement: Stability and estimations of size*, SIAM J. of Math. Anal. **28** (1997), 1389–1405.

[19] O. Kwon and J. K. Seo, *Total size estimation and identification of multiple anomalies in the inverse electrical impedance tomography*, Inverse Problems **17** (2001), 59–75.

[20] O. Kwon, J. K. Seo, and J. R. Yoon, *A real time algorithm for the location search of discontinuous concuctivites with one measurement*, submitted for publication.

[21] ———, *Inverse conductivity problem: Local search method for multiple anomalies*, in preparation.

Ohin Kwon
Department of Mathematics and Natural Science
Research Institute
Yonsei University
Seoul 120-749, Korea
E-mail: oikwon@math.snu.ac.kr

Jin Keun Seo
Department of Mathematics
Yonsei University
Seoul 120-749, Korea
E-mail: seoj@bubble.yonsei.ac.kr

Eung Je Woo
School of Electronics and Information
Kyung Hee University
Kyungki 449-701, Korea
E-mail: ejwoo@khu.ac.kr

Jeong-Rock Yoon
School of Mathematics
Korea Institute for Advanced Study
Seoul 130-012, Korea
E-mail: jryoon@numer.kaist.ac.kr